Journal of Operation and Automation in Power Engineering
Vol. 11, No. 3, Oct.. 2023, Pages: 213-222
http://joape.uma.ac.ir

High Gain DC/DC Converter Implemented with MPPT Algorithm for DC Microgrid System

E. Naderi, S.J. Seyedshenava, H. Shayeghi*

Energy Management Research Center, University of Mohaghegh Ardabili, Ardabil, Iran

Abstract- *This paper presents the output voltage control and execution of a novel non-isolated high step-up (NIHS) DC-DC converter connected to a solar photovoltaic (PV) based DC microgrid system. The proposed converter provides a high output voltage conversion ratio over smaller duty cycles, small inductors, low cost, and high efficiency to enhance the level of the generated voltages of PV. Also, to overcome the drawback of PV, the detailed operation of maximum power point tracking (MPPT) for the novel boost DC-DC converter topology is presented. A control algorithm, modified perturb and observe (MP&O), is put forward to assure that the maximum power is extracted from PV at any environmental condition. It regulates the output voltage of the PV system to the desired DC bus voltage. This technique is compared with the Incremental Conductance (INC) and conventional P&O algorithm in terms of their computational complexity and oscillations near maximum power point (MPP) using MATLAB & Simulink. The focus is on the continuous conduction mode of the proposed converter. To demonstrate the effectiveness of the proposed converter, operation modes, and technical analysis are conducted. Also, the experimental results of a 200 W-12V/120V, 25 kHz prototype are given and discussed to justify the suggested converter.*

Keyword: High Step-up Boost Converter, Switched-Inductor, DC Microgrid, Maximum power point tracker (MPPT), Perturb and Observe (P&O) technique, Incremental Conductance (INC).

NOMENCLATURE

CCM	Continuous conduction mode
CSIBC	Conventional SIBC
CCMP&O	Current control modifier perturbation and observation
DC	Direct current
EV	Electric vehicle
FOCV	Fractional open circuit voltage
INC	Incremental conductance
IBC	Interleaved boost converter
MP&O	Modified perturb and observe
MPPT	Maximum power point tracker
MPP	Maximum power point
MSCBC	Modified switched capacitor boost cell
MSIBC	Modified switched inductor boost cell
NIHS	Non-isolated high step-up
P&O	Perturb and observe
SC	Switched capacitor
SI	Switched inductor
SCC	Switched capacitor converter
SIC	Switched inductor cell
SIBC	Switched inductor boost cell

Received: 03 Feb. 2022
Revised: 19 Feb. 2022
Accepted: 22 May 2022
*Corresponding author: (S.J. Seyedshenava)
E-mail: seyedshenava@uma.ac.ir
DOI: 10.22098/joape.2023.10270.1731
Research Paper

1. INTRODUCTION

Recently, direct current (DC) microgrids gained more concentration because of the high efficiency, uncomplicated interconnection of renewable sources, and increase in DC loads. The merits and features such as reducing the negative impact of fast charging of EVs on the power grid, higher reliability, and efficiency, simple control strategies and no need for synchronization due to the absence of frequency are incentives for the researchers and industries to research and investment in the DC-microgrids. Also, DC Microgrid has a promising future due to its better adaptability with PVs and fuel cells. Among renewable energy sources, solar PV plays a crucial role in DC microgrid systems for its high reliability, non-polluting, and minimum maintenance and cost. PV systems are a free, infinite, and environmentally friendly energy source. Also, it requires comparatively low maintenance, and it has a long life span compared to other renewable sources [1], [2]. As a result, it has become a popular way of generating electricity. However, low conversion efficiency, high power generated cost, and intermittency are the main drawbacks of solar PV modules. The conversion efficiency is less than 17% and the output power of PV cells changes with weather conditions [3].

Furthermore, the characteristics of PV cells (I-V or V-P) are not linear and depend on insolation and temperature. Therefore, to ensure that the maximum power is extracted from the PV panels, an MPPT controller is required. The dynamic response speed of MPPT is crucial under some instantaneous environmental conditions changing. Because of this, numerous techniques such as traditional and intelligent control algorithms have been proposed in the literature.

Perturb & Observe (P&O), Incremental Conductance (INC), the constant voltage, Fractional Open Circuit Voltage are the traditional control methods. In contrast, artificial neural networks, particle swarm optimization, and fuzzy-logic [4-5] are the intelligent methods which artificial neural networks (ANN) and fuzzy logic (FL) techniques are the most widely used MPPT methods in the literature [6]. These methods are very sensitive and consume significant computational resources. Intelligent methods perform exceptionally well in nonlinear systems [7]. The most common MPPT algorithms are INC and P&O due to their high accuracy, simplicity and rapid response time. INC MPPT algorithm with integral regulator has been proposed in [8] to maintain the system's response more rapid and accurate. A PV system with MPPT based on self-predictive incremental conductance (SPInC) has been developed in [9]. SPInC algorithm outperforms the classical INC, and the output power has a minimal ripple. In [10] the algorithm of CCMP&O−FLC MPPT has been applied to reduce the setting time and to reduce oscillation around the set-point at a steady state.

Also, power electric converters are the core part of PV sources. DC-DC converter role is the extraction of the maximum available power from the PV panels by controlling the switching devices in this converter [11]. The design and manufacture of converters with essential criteria such as high efficiency, high voltage gain, simple structure and control, and low voltage stress on switches and diodes, are performed by researchers and industries. In conventional boost converter high voltage gain can be achieved by adjusting the duty cycle which creates high voltage stress on switch and high inductor current ripples. Also, it creates high conduction loss which impacts on the conversion efficiency. Accordingly, many different isolated and non-isolated DC-DC converter topologies addressed with utilizing an SC, SI, Z source, Y-Source, voltage multiplier, and Quasi Z source for unidirectional and bidirectional DC-DC converters. The NIHS DC-DC converter configurations due to higher conversion ratios, high power, low volume, low weight, and low voltage stress across switches replace the conventional DC-DC converters and isolated converters. For increasing the voltage gain at a limited duty cycle in the non-isolated converter, coupled inductor [12], Interleaved Boost Converters (IBCs) [13], switched capacitor converter (SCC) [14-15], switched inductor cell (SIC) [16-17], quadratic boost converter [18-19], multilevel boost converter [20] are recommended. Each of these converters has its specific merits and demerits, depending on the operating circumstances and specifications. Boost converters integrated with switched inductor boost cells (SIBC) and switched capacitor (SC) are convenient ways to increase the output voltage gain [21-23]. In [22] voltage stress across active switches has been reduced and in [23] voltage gain has been improved in low duty cycle. However, the main disadvantage of these converters are its complicated control algorithm and these modifications have not led to a significant increase in voltage gain. Also, the voltage regulation and efficiency of these converters is not acceptable [21], [22]. By integration of SC circuit with coupled inductor converters in [23], the discontinuous input current has been removed. However, an additional passive clamp circuit must be added to eliminate the leakage inductive energy of the coupled inductors, which causes voltage spikes on the semiconductors. In [24, 25] the integration of SI and SC converters has been reported. It results in enhancing the voltage conversion ratio and reducing the voltage stress on the devices. However, its practical applications are restricted by high output ripple and a large number of semiconductors.

Therefore, this article suggests incorporating the modified switched capacitor boost cell (MSCBC) and MSIBC. In the proposed DC-DC converter, inductors in MSIBC leads to improve voltage gain and reduction of voltage stress on the switch and diodes. The energy stored in the inductor is used to charge the capacitors in parallel when the switch is OFF. Therefore, the regulated output voltage can be obtained by adjusting the voltage of capacitors. Also, in this topology, power diodes turn ON and OFF softly in the zero current switchings (ZCS) condition. Therefore, the reverse recovery loss of diodes is decreased. The efficiency has been enhanced by decreasing reverse recovery losses in the diodes. The high voltage gain capability (about 13 at a nominal duty ratio of D=0.6) has been achieved by applying different gain expansion methods in the proposed converter. Based on the literature review and the problems with PV panels and traditional boost converters, this paper presents the configuration and

investigation of an efficient DC-DC boost converter with MPPT technology. The performance of solar module at 500W/m2 solar insolation and 25°C ambient temperature is analysed. P&O, Modified P&O (MP&O) and INC methods are executed and evaluated.

The arrangement of this article is as follows: Section 1 presents a comprehensive introduction to the suggested idea. In Section 2, the power converter configuration and technological specifications of the presented converter are explained. The main circuit parameter design and voltage stress analysis are presented in sections 3 and 4, respectively. The Performance of MPP Execution has been conducted in Section 5. The comparison of the INC, P&O, and MP&O results and experimental results from a prototype converter are explained in Section 6.

2. POWER CONVERTER CONFIGURATION

The basic structure of solar fed NIHS DC-DC converter for DC micro grid applications is shown in Fig. 1. The topology of the conventional SC is modified to overcome the problem of high voltage stress and power losses on the diodes. The elements of this topology are one active semiconductor switch (Q), five diodes, five passive capacitors, three passive inductors, one output diode, and one output capacitor. The MSIBC is formed by the composition of L_1, L_2, D_1, D_2, and C_B. The boost capacitor (C_B) in the MSIBC topology causes voltage stress reduction on semiconductors and increases the voltage gain [16]. The MSCBC is formed by the composition of switched capacitors (C_1, C_2, C_3, and C_b), switched capacitor diodes (D_{c1}, D_{c2}, and D_b). Inductor energy storage cell (L_2) to provide energy for C_b and C_2.

2.1 Continuous conduction mode (CCM)

In analyzing CCM mode, all elements are considered ideal for an easier understanding of the converter operation. Also, the characteristics of waveforms during this mode are shown in Fig. 2. The equivalent circuits of the proposed converter in CCM is shown in Fig. 3.

Mode I: Switch Q is ON: By applying the signal to the gate of MOSFET Q, it starts to conduct. D_1 and D_2 diodes become forward biased and help to parallel charge of MSIBC elements (L_1, L_2, C_B). Therefore, voltage source V_{in} supplies energy to the inductor L_1, L_2, and capacitor C_B. Simultaneous, C_3 charges C_b and L_b. Meanwhile, C_1 and C_2 are in series with C_3, diode D_o is ON and charging current starts to flow charging up C_o. Finally, C_o supplies energy to the load R_L. The topological specification of this mode is shown in Fig. 3(a). When the Q, D_1, D_2 are ON, L_1, L_2, and C_B are parallel. Hence, the voltage of L_1, L_2, C_B, and the output capacitor can be expressed as follows:

$$V_{in} = V_{L_1} = V_{L_2} = V_{C_B} \tag{1}$$

$$V_{C_o} = V_{out} = V_{C_1} + V_{C_2} + V_{C_3} \tag{2}$$

Mode II: Switch Q is OFF: Fig. 3(b) shows the topological specification of mode II. In MISBC, diodes (D_1 and D_2) are reserved biased. The inductors (L_1, L_2) and capacitor (C_B) are connected in series and discharged to MSCBC capacitors (C_1, C_2, C_3). Fig. 2(a) shows the voltage of switch and current of inductors. As the voltage of C_b and C_2 are equal before the switch conducts, during this mode voltage of C_b is more than C_2. Therefore, diode D_{c1} and D_{c2} conducts and D_b remains OFF. D_{c1} is turned ON at ZCS condition and D_{c2} turned OFF at zero current, as shown in Fig. 2(b). L_b charges C_2 via D_{c1} and also C_b discharges. When V_{c2} increases to V_{cb}, D_b conduct, and L_b charges C_2 and C_b in parallel; thus, their voltage will be equal. D_o is reversed bias during this mode of operation. At steady state, according to the volt-second balance principle on L_1 and L_b, we have

$$\int_0^{DT_s} V_{in} = \int_{DT_s}^{T_s} \left(-V_{in} + \frac{V_{C_1}}{2}\right) = \int_{DT_s}^{T_s} \left(-V_{in} + \frac{V_{C_3}}{2}\right) \tag{3}$$

$$\int_0^{DT_s} \left(V_{C_3} - V_{C_b}\right) = \int_{DT_s}^{T_s} \left(V_{C_b}\right) \tag{4}$$

Then, the voltage of C_1 and C_2 are obtained as follow:

$$V_{C_1} = V_{C_1} = \frac{2V_{in}}{1-D} \tag{5}$$

$$V_{C_b} = V_{C_2} = V_{C_3} D \tag{6}$$

Thus, C_1, C_2, and C_3 are in series to supply the load when Q is on. Therefore, the voltage gain of the converter can be derived as:

$$G_{CCM} = \frac{V_o}{V_{in}} = \frac{4+2D}{1-D} \tag{7}$$

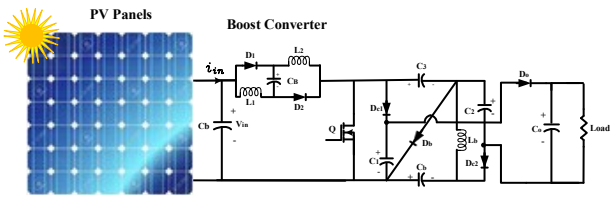

Fig. 1. The topology of the proposed converter

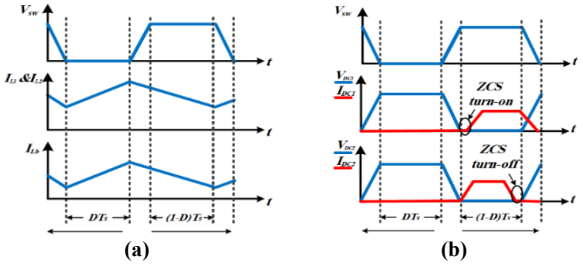

Fig. 2. (a)-(b) The characteristics waveform in CCM

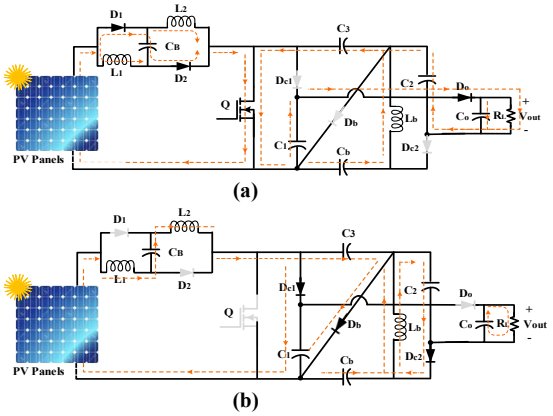

Fig. 3. (a)-(b) equivalent circuits during CCM

3. PARAMETER DESIGN GUIDELINE

3.1. Magnetic elements selection

In the case of a boost inductor, the maximum current ripple (ΔI_L) is limited to 20% of the maximum average inductor current. In the proposed converter, inductors are chosen dependent on the current ripple and switching frequency:

$$L_1 = L_2 = \frac{V_{in} D}{\Delta I_L f_s} \tag{8}$$

$$L_b = \frac{2V_{in} D}{\Delta I_L f_s} \tag{9}$$

3.2. Capacitor selection

The selection of capacitors is based on the voltage ripple (ΔV_C) and switching frequency. The size of the output capacitor is derived as given in Eq. (10).

$$C_o = \frac{V_o (1-D)}{R_L f_s \Delta V_{c_o}} \tag{10}$$

The values of switched capacitors C_1, C_2, and C_B are as follow:

$$C_1 = \frac{V_o}{R_L f_s \Delta V_{c_1}} \tag{11}$$

$$C_2 = \frac{V_o}{R_L f_s \Delta V_{c_2}} \tag{12}$$

$$C_B = \frac{(2+D) V_o}{R_L f_s \Delta V_{c_B}} \tag{13}$$

Also, C_b and C_3 are calculated by the following equation.

$$C_b = \frac{DI_o}{f_s \Delta V_{c_b}} = \frac{DV_o}{R_L f_s \Delta V_{c_b}} \tag{14}$$

$$C_3 = \frac{(1+D) V_o}{R_L f_s \Delta V_{c_3}} \tag{15}$$

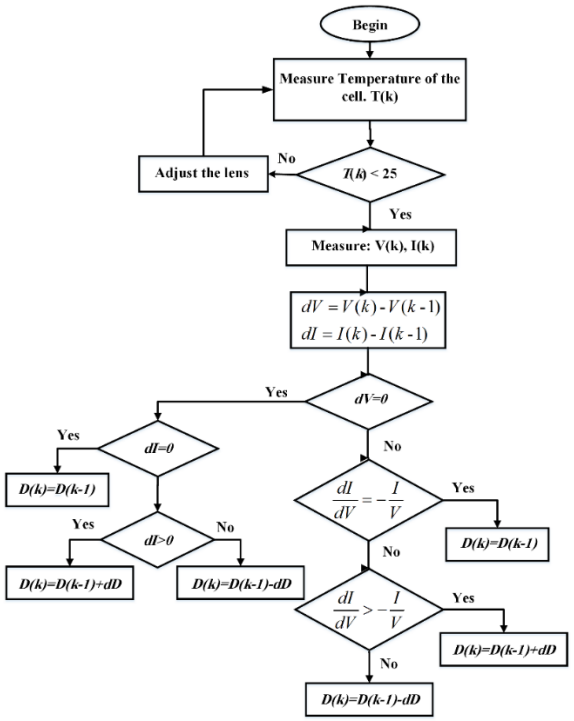

Fig. 4 Flowchart of the Improved INC Algorithm

4. VOLTAGE STRESS ANALYSIS

The voltage stress must be determined to choose the proper power switch and diodes. The voltage stresses of the switch (Q) during CCM operation can be expressed as:

$$V_{stress-Q} = \frac{2V_o}{(4+2D)}, T_{ON} \le t \le T_s \tag{16}$$

The voltage stress of diodes is calculated as given in (17)–(20):

$$V_{stress-D1} = V_{stress-D2} = \frac{V_o}{(4+2D)}, T_{ON} \le t \le T_s \tag{17}$$

$$V_{stress-DC1} = V_{stress-DC2} = \frac{2V_o}{(4+2D)}, 0 \le t \le T_{ON} \tag{18}$$

$$V_{stress-D0} = \frac{2V_o}{(4+2D)}, T_{ON} \le t \le T_s \tag{19}$$

$$V_{stress-Db} = \frac{2V_o}{(4+2D)}, 0 \le t \le T_{ON} \tag{20}$$

5. PERFORMANCE OF MPP EXECUTION

5.1. INC strategy

One of the most important power generations is PV cells. These sources are made from layers or sheets of silicon, which change the sunlight into power electricity. The PV cells are connected in parallel and series to generate high voltage. However, PV systems need a boost converter to increase their output voltage. Also, the MPPT algorithm is used to extract the maximum

power of these panels. INC strategy, one of the most widely used MPPT methods, calculates the maximum power by comparing the instantaneous conductance and the change in conductance of photovoltaic cells. In comparison to P&O's algorithm, this method involves more computation but can follow condition variation more quickly. In this method, the power characteristic slope of the solar cell is used. Three regions are defined in the power curve considering the curve slope [26]. The INC method relies on the following equations.

$$\frac{dP}{dV} > 0 \Rightarrow \frac{dI}{dV} > -\frac{I}{V} \tag{21}$$

$$\frac{dP}{dV} = 0 \Rightarrow \frac{dI}{dV} = -\frac{I}{V} \tag{22}$$

$$\frac{dP}{dV} < 0 \Rightarrow \frac{dI}{dV} < -\frac{I}{V} \tag{23}$$

The flowchart of INC strategy is presented in Fig. 4.

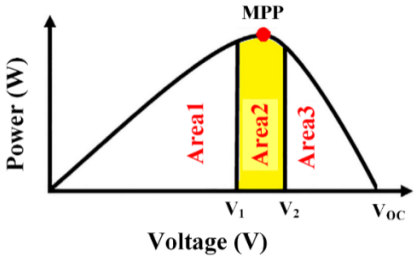

Fig. 5 Power curve search space limitation

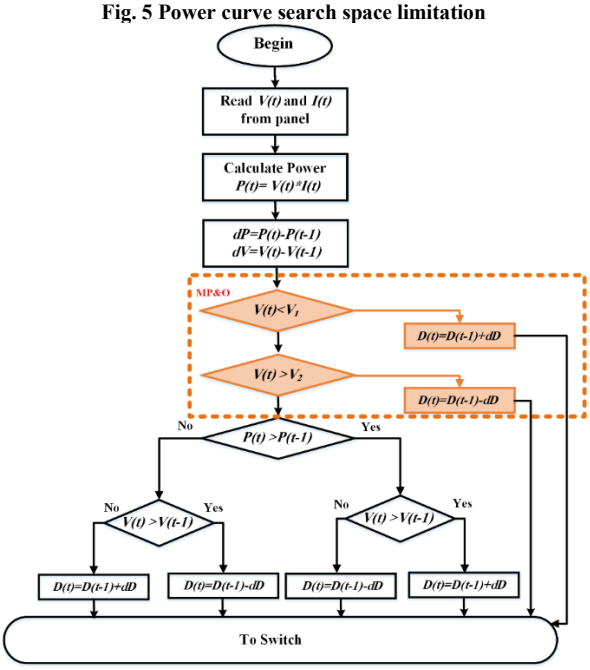

Fig. 6 Flowchart of the MP&O Algorithm

5.2. P&O and Modified P&O strategy

The PV module's power is varied by introducing a minor perturbation to the system in this algorithm. The previous power is compared with the measured output power of PV. If the output power raises, the process is repeated, otherwise the perturbation is inverted. PV module voltage is increased or decreased to determine whether power is increasing or decreasing. Power increases when voltage goes up, which means the PV module has its operating point on the left-hand side of the MPP. However, further perturbation on the right hand side is necessary in order to reach MPP. If, on the other hand, a voltage increase causes a power drop, this indicates that the PV module is operating on the right hand of the MPP. To reach the MPP, further perturbations are needed to the left. The P&O algorithm has also been modified by numerous researchers to address the response time problem and steady state oscillations [27]. MP&O restricts the search space only about 10% of the power curve, which reduces response time and minimizes steady-state oscillations. Fig. 5 shows the P-V curve separated into three regions named area 1, area 2 and area 3. Area 2 contains the maximum power point within a region containing only 10% of the PV curve, and the improved algorithm must search only within area 2 to find the maximum power point. Therefore, the algorithm's step response time can be reduced and steady state oscillations about the MPP can be eliminated. The modification in P&O algorithm is shown in Fig. 6.

6. EXPERIMENTATION TEST RESULTS

The effectiveness of the proposed converter has been verified by experimental results. Also, to harvest maximum power from the PV panel three MPPT method is implemented and tested by Simulink/MATLAB software. The structure of NIHS DC-DC converter, a PV unit and an MPPT controller is shown in Fig. 7. The proposed PV system, P–V, and the I–V characteristics are shown in Fig. 8. The INC, P&O and MP&O techniques are used for the MPPT function. Therefore, the switching state for the proposed DC-DC converter generates by the MPPT methods. The results of three methods are compared with each other. The circuit specifications and components are given in Table 1. Mathematical models for solar panels were constructed based on conditions of 500W/m2 solar radiation and 25°C ambient temperatures. The simulations examined the converter's static and dynamic behavior.

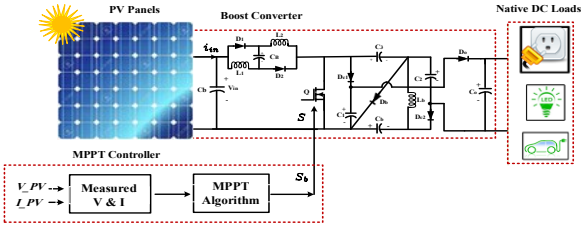

Fig. 7. The topology of the proposed converter

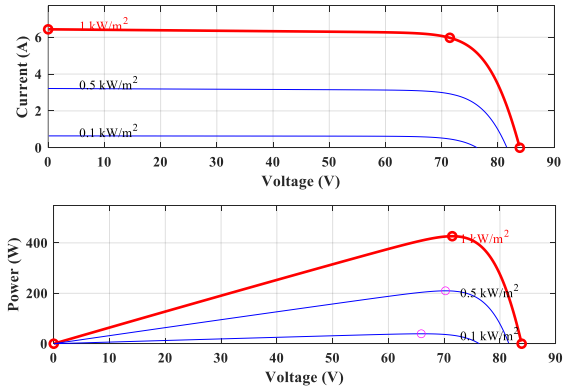

Fig. 8. P–V and I–V characteristics at 25 °C temperature

Table 1 The circuit specifications and components

parameters	specifications	parameters	specifications
Output power	200 w	Inductor L_b	470uH
Input voltage	12 V	Switch	IRFP260NPBF
Output voltage	120 V	Diodes	RHRG15120
Input Current	16.67 A	Diodes	FFPF30U60S
Output Current	1.67 A	Capacitor C_B	220uF
Switching frequency	25 kHz	Capacitor C_2, C_b	220 uF
Duty cycle	0.52	Capacitor C_O	680 uF
Inductors, L_1,L_2	220 uH	Capacitors C_1, C_3	220uF

6.1. Comparison of converter Behavior under Different MPPT strategy

This section is devoted to presenting and discussing the comparison simulation results. The comparison of converter behaviour under Different MPPT strategy has been studied to investigate the effectiveness of the presented MPPT procedure. The output voltage of PV and the boost converter and its zoomed version for the mentioned strategies are shown in Fig. 9-11 (a) and (b). Also Fig. 12 (a) -(c) shows the output power of the proposed DC-DC converter and its zoomed version for the mentioned MPPT algorithms.

As can be seen, the mentioned strategies can achieve maximum power point tracking. The INC method finds the maximum power point faster than the P&O strategy. However, the simulation outcomes of the MP&O MPPT techniques can achieve the maximum power point tracking more quickly. Fig. 9 shows the smooth output of the INC algorithm which tracks the maximum power point by eliminating steady state oscillations about the MPP. In MP&O method the oscillation is smaller and the accuracy is higher than P&O strategy. The simulation results indicate the superior performance of the MP&O compared to the INC and P&O techniques in effectively and efficiently tracking the MPP with the high speed. The INC technique has the least steady-state oscillation at the MPP but this method involves more computation. Also, MP&O was simulated under varying atmospheric conditions such as irradiance to ensure successful implementation. The power output of PV under fluctuating solar irradiance is presented in Fig. 13. In different steps, the solar irradiance was varied from 500 W/m2 to 100 W/m2. Both uniform and variable atmospheric conditions were correctly followed by the MP&O algorithm with a very low steady-state oscillation at the MPP. Under changing atmospheric conditions, the conventional P&O can lose the locus point due to so many oscillations at the MPP.

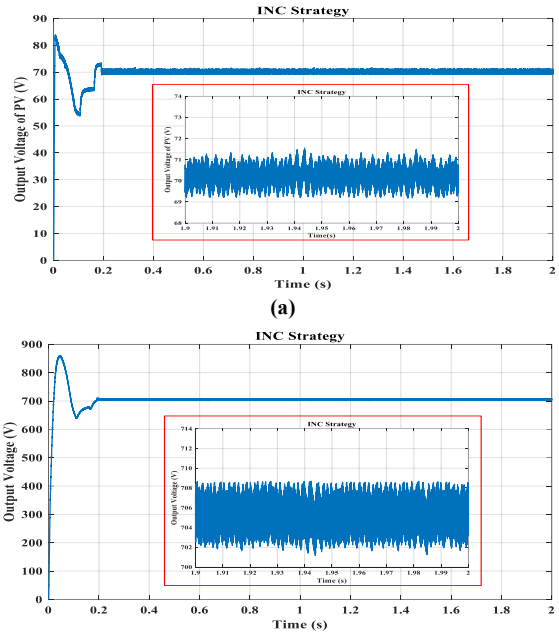

Fig. 9. INC MPPT method results (a) output voltage of PV (b) output voltage of the proposed converter

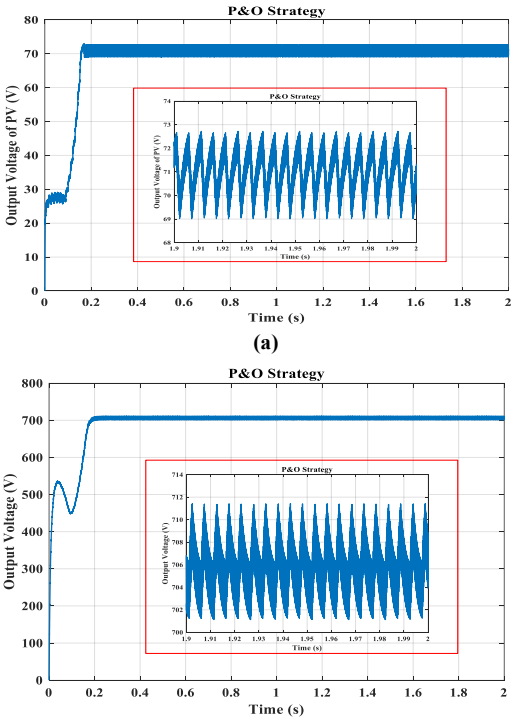

Fig. 10. P&O MPPT method results (a) output voltage of PV (b) output voltage of the proposed converter

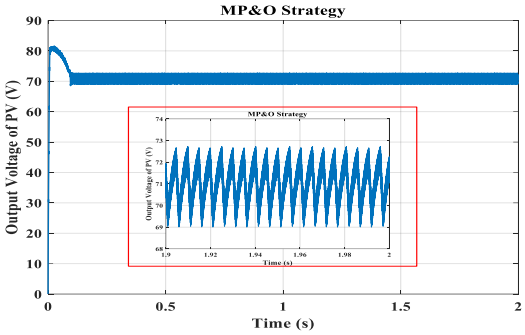

(a)

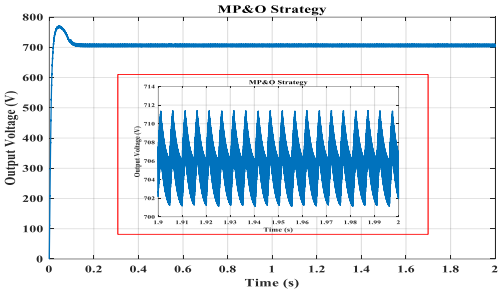

(b)

Fig. 11. MP&O MPPT method results (a) output voltage of PV (b) output voltage of the proposed converter

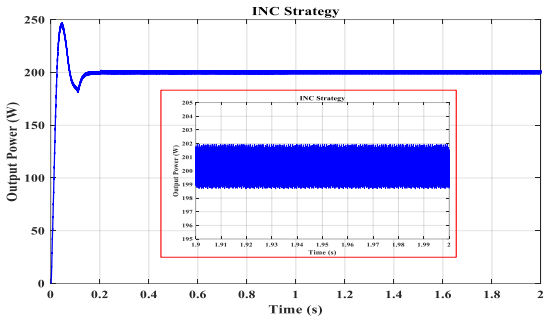

(a)

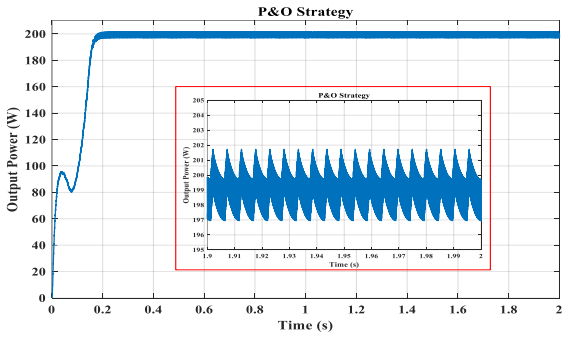

(b)

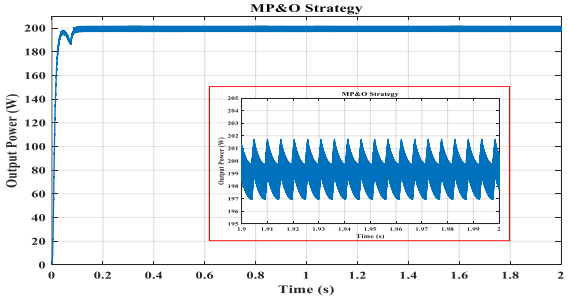

(c)

Fig. 12. The output power (a) INC (b) P&O (c) MP&O MPPT method

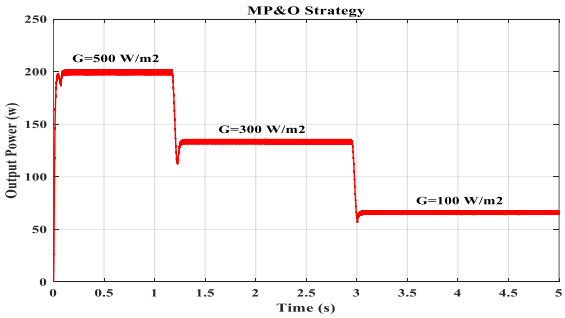

Fig. 13. MP&O MPPT result under varying atmospheric weather conditions

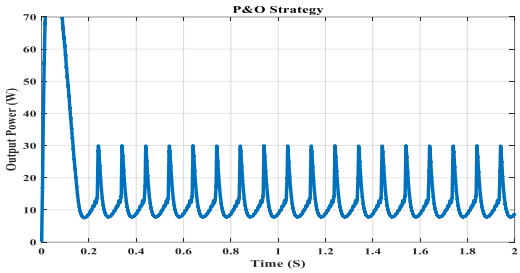

(a)

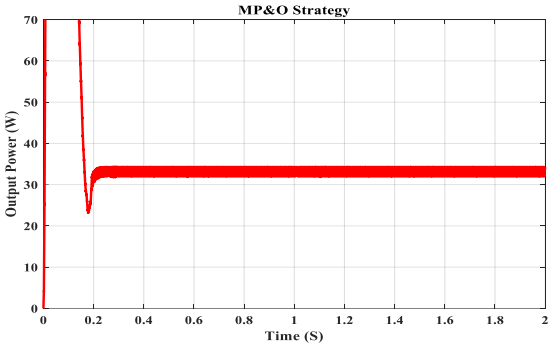

(b)

Fig. 14. MPPT result under lower irradiances (G<100W/m2), (a) P&O (b) MP&O Strategy

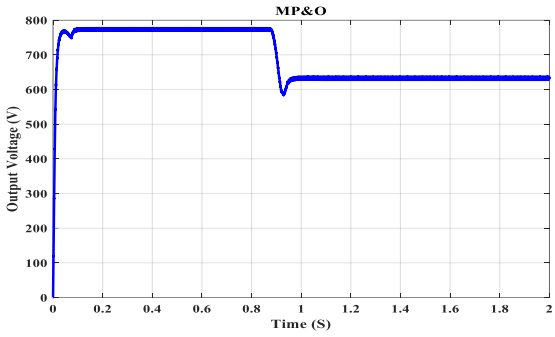

Fig. 15. MP&O MPPT result under varying the reference DC bus voltage

As shown in Fig.14, MP&O can correctly follow in lower irradiances with a very low steady-state oscillation at the MPP but P&O couldn't exactly detect the location of MPP. Also, if the value of the reference DC bus voltage changes MP&O can track the new reference value. Fig. 15 shows the output voltage of the boost converter under varying the reference DC bus voltage.

6.2 Experimentation test results

Fig. 16 shows the photograph of the implemented prototype. The control circuit includes ATMEGA8 to control and generate switching signals and IR2110 to drive low side MOSFET. Fig. 17-20 shows the experimental results of the presented converter. Fig. 17(a) shows output voltage of the hardware prototype. Based on this diagram, 120 V output voltage is obtained when the duty cycle is about 0.52 and V_{in} is 12 V. This diagram proves the obtained conversion ratio in Eq. (7). Also, there is a low output voltage ripple.

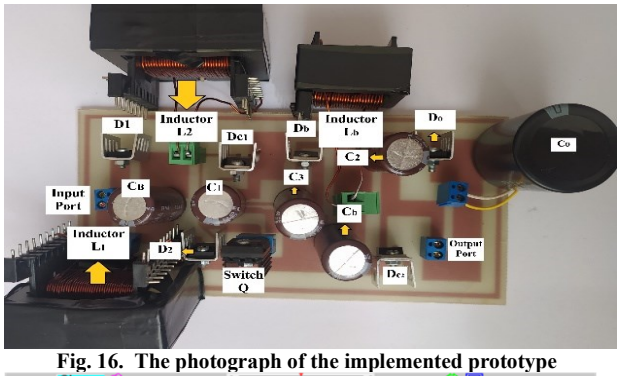

Fig. 16. The photograph of the implemented prototype

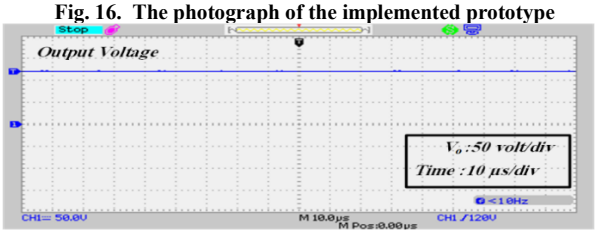

(a)

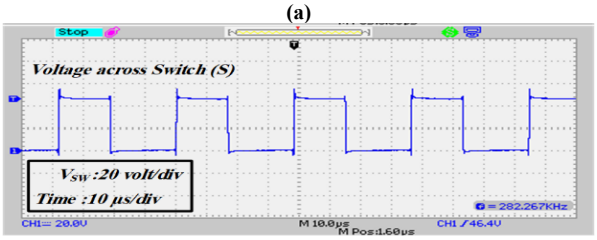

(b)

Fig. 17. The waveforms of (a) the output voltage (b) the voltage across switch Q

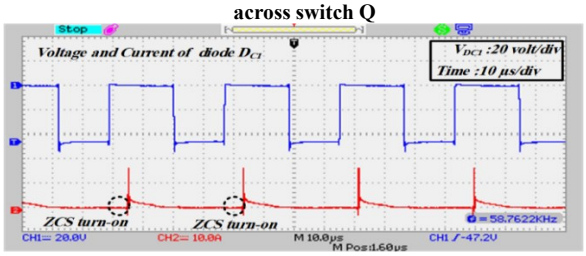

(a)

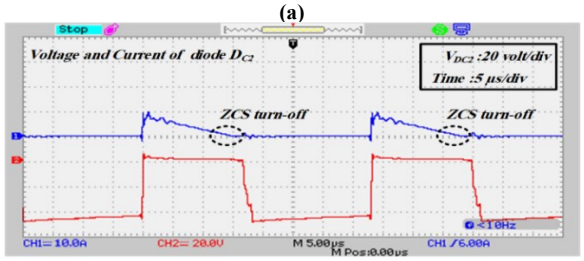

(b)

Fig. 18 (a) The voltage and current of DC_1. (b) The voltage and current of DC_2

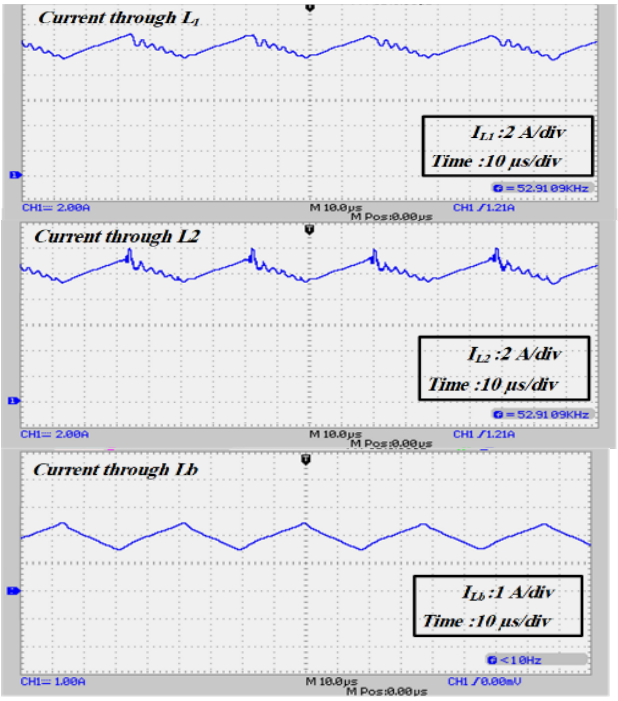

Fig. 19. The current of inductors L_1, L_2, and L_b.

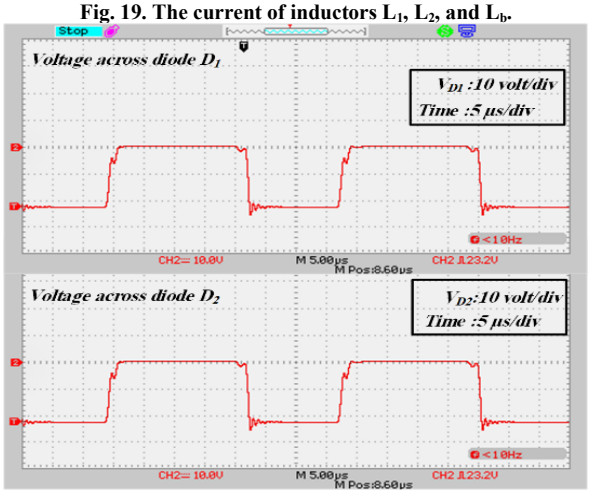

(a)

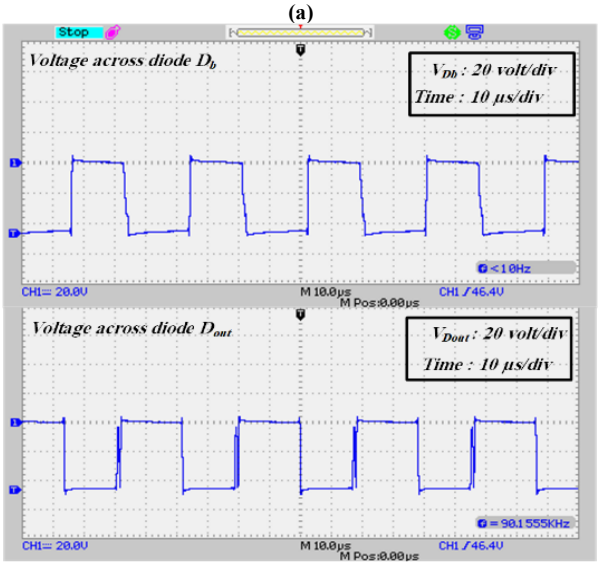

(b)

Fig. 20. (a) The voltage across diodes D_1 and D_2. (b) The voltage across D_b and D_{out}

Table 2 The experimental results

Parameters	Values
V_{out}	120 V
V_{D1}	24 V
V_{D2}	24 V
V_{Db}	43 V
V_{Dout}	43 V
V_{SW}	43 V

The voltage across active switch Q is presented in Fig. 17 (b). It shows that the voltage across the active switch Q is less than half of the output voltage. It confirms the theoretical analysis. The voltage and current of switched capacitor cell diodes D_{C1} & D_{C2} are shown in Fig. 18. Diodes D_{C1} and D_{C2} are turned on and OFF under ZCS conditions that cause a reduction of the reverse recovery loss and enhance efficiency. The maximum voltage of switched capacitor diodes is almost 47V and approximately the third of the output voltage. Fig. 19 demonstrates the conducting current through the inductances L_1, L_2, and L_b. The inductors L_1 and L_2 are simultaneously charged and discharged, and their average currents are 9.3 A. The percentage ripple of the current throughout the inductors is close to the desired value, and it is low. The experimental results of the diodes D_1, D_2, D_b and output diode D_o are presented in Fig. 20 and Table. 2, which is essentially compatible with the theoretical computation. The voltage stress of the diodes D_1 and D_2 is nearly 24V, which is lower than a quarter of the output voltage. The proposed structure seems to be an acceptable choice for sustainable and renewable energies based on the theoretical analysis and experimental results. Some of the most important parameters like the high voltage gain and low voltage stresses across the semiconductors are considerably more beneficial. These parameters were achieved by the integration of MSCBC and MSIBC specifications. These terms ensure the reliability of the topology and cause the converter to be ready for DC microgrid applications such as PV.

7. CONCLUSION

This work aims to develop an innovative NIHS DC-DC converter whose duty cycle is controlled to extract maximum power from PV by modified P&O algorithm. High voltage gain, the low voltage stress on the switch and diodes, and ZCS are the main novelty of the presented converter. This converter can execute control algorithms efficiently because only a single active switch is used. Various MPPT strategies, namely, P&O, INC, and MP&O with a proposed converter have been discussed in detail. The MPPT strategies were tested and validated with the MATLAB/Simulink software. In terms of maximum power extraction, MP&O-based MPPT controllers provide better results than P&O and INC-based controllers. The MP&O controller is characterized by a smaller settling time, along with fewer steady state oscillations, when compared to P&O and INC controllers. Under changing atmospheric conditions, the MP&O can follow the locus point due to low oscillations at the MPP. The proposed converter and MPPT strategy exhibit noticeable characteristics that make them an excellent selection for boosting low voltage from solar PV and to high voltage for DC microgrids. The experimental results of a 200 W prototype were also discussed to justify the suggested converter.

REFERENCES

[1] S. Mohamed, M. Abd El Sattar, " A comparative study of P&O and INC maximum power point tracking techniques for grid-connected PV systems", *SN Applied Sciences*, vol. 1, no. 2, pp.174, 2019.

[2] E. Naderi et al, "MILP based optimal design of hybrid microgrid by considering statistical wind estimation and demand response", *J. Oper. Autom. Power Eng.*, vol. 10, no. 1, pp 54-65, 2022.

[3] S. Salman, X. AI, W. Zhouyang, "Design of a P-&-O algorithm based MPPT charge controller for a stand-alone 200W PV system, *Protect. Control Modern Power Syst.*", no.1, pp. 1-8, 2018.

[4] S. Babaa et al., "Overview of maximum power point tracking control methods for PV systems", *J. Power Energy Eng*, vol. 2, no. 8, pp.59-72, 2014.

[5] P. Cheng et al., "Optimization of a fuzzy-logic-control-based MPPT algorithm using the particle swarm optimization technique", *Energies*, vol. 8, no. 6, pp. 5338-5360, 2015.

[6] M. Guerra, F. Ugulino, D. Araújo, "Assessing maximum power point tracking intelligent techniques on a PV system with a buck–boost converter", *Energies*, vol. 14, no. 22, pp. 7453, 2021.

[7] G. Giurgi, L. Szolga, D. Giurgi, "Benefits of fuzzy logic on MPPT and PI controllers in the chain of photovoltaic control systems", *Appl. Sci.*, vol. 12, pp. 2318, 2022.

[8] M. Siddique et al., "Implementation of incremental conductance MPPT algorithm with integral regulator by using boost converter in grid-connected PV array." IETE *J. Res.*, pp.1-14, 2021.

[9] S. Zand et al., "Improvement of self-predictive incremental conductance algorithm with the ability to detect dynamic conditions", *Energies*. vol. 14, no. 5, pp. 1234, 2021.

[10] A. Aurairat and B. Plangklang, "An alternative perturbation and observation modifier maximum power point tracking of PV systems", *Symmetry*, vol.14, no. 1, pp. 44, 2021.

[11] P. Sharma and V. Agarwal, "Maximum power extraction from a partially shaded PV array using shunt-series compensation", *IEEE J. Photovoltaic,* vol. 4, no. 4, pp. 1128-37, 2014.

[12] N. Abouchabana et al., "Power efficiency improvement of a boost converter using a coupled inductor with a fuzzy logic controller: application to a photovoltaic system", *Appl. Sci.*, vol. 11, no. 3, pp. 980, 2021.

[13] A Garrigós et al., "Interleaved, switched-inductor, multi-phase, multi-device DC/DC boost converter for non-

isolated and high conversion ratio fuel cell applications", *Int. J. Hydrogen Energy*, vol. 44, pp. 12783-92, 2019.

[14] V. Tran et al., "Switched-capacitor-based high boost DC-DC converter", *Energies*, vol. 11, no. 4, pp 987, 2018.

[15] Q. Qi, D. Ghaderi, J. Guerrero. "Sliding mode controller-based switched-capacitor-based high DC gain and low voltage stress DC-DC boost converter for photovoltaic applications", *Int. J. Electr. Power Energy Syst.*, vol. 125, pp. 106496, 2021.

[16] Y. Tang, T. Wang, D. Fu, "Multicell switched-inductor/ switched-capacitor combined active-network converters", *IEEE Trans. Power Electron.*, vol. 30, pp 2063-72, 2014.

[17] G. Shokri, E. Naderi, S. SeyedShenava, "Active and reactive power control of grid-connected PV power systems based on HGNISS DC-DC converter and SMDPC strategy", *Power Electron. Drive Syst. Tech. Conf.*, 2020.

[18] G. Li et al., "A novel quadratic boost converter with low inductor currents", *Trans. Power Electron. Appl.*, vol. 5, no. 1, pp 1-10, 2020

[19] S. Srinivasan et al., "Neural network based MPPT control with reconfigured quadratic boost converter for fuel cell application", *Int. J. Hydrogen Energy*, vol. 46, no. 9, pp. 6709-19, 2021.

[20] N. Osman, M. Mohamad Elias, N. Abd Rahim, "Three-level hybrid boost converter with output voltage regulation and capacitor balancing", *IETE J. Res.*, pp 1-9, 2021.

[21] B. Axelrod, Y. Berkovich, A Ioinovici, "Switched-capacitor/switched-inductor structures for getting transformerless hybrid DC–DC PWM converters", *IEEE Trans. Circuits Syst. I: Regular Papers*, vol. 55, no. 2, pp 687-96, 2008.

[22] S. Sadaf et al, "A novel modified switched inductor boost converter with reduced switch voltage stress", *IEEE Trans. Ind. Electron.*, vol. 68, no. 2, pp 1275-89, 2020.

[23] B. Faridpak et al., "Improved hybrid switched inductor/switched capacitor DC–DC converters", *IEEE Trans. Power Electron.*, vol. 36, no. 3, pp 3053-62, 2020.

[24] M. Bhaskar et al., "Modified multilevel buck–boost converter with equal voltage across each capacitor: Analysis and experimental investigations", *IET Power Electron.*, vol. 12, no. 13, pp 3318-3330, 2019.

[25] H. Xie, R. Li, "A novel switched-capacitor converter with high voltage gain", *IEEE Access,* no. 7, pp 107831-107844, 2019.

[26] H. Shahid et al., "Implementation of the novel temperature controller and incremental conductance MPPT algorithm for indoor photovoltaic system", *Solar Energy,* vol. 163, pp. 235-242, 2018.

[27] M. Kamran et al, "Implementation of improved Perturb & Observe MPPT technique with confined search space for standalone photovoltaic system", *J. King Saud Uni. Eng. Sci.*, vol. 32, no. 7, pp. 432-41, 2020.